



HAL
open science

Time-of-day-dependent variation of the human liver transcriptome and metabolome is disrupted in MASLD

Manuel Johanns, Joel T Haas, Violetta Raverdy, Jimmy Vandel, Julie Chevalier-Dubois, Loic Guille, Bruno Derudas, Benjamin Legendre, Robert Caiazzo, Helene Verkindt, et al.

► To cite this version:

Manuel Johanns, Joel T Haas, Violetta Raverdy, Jimmy Vandel, Julie Chevalier-Dubois, et al.. Time-of-day-dependent variation of the human liver transcriptome and metabolome is disrupted in MASLD. *JHEP Reports Innovation in Hepatology*, In press, 6 (1), pp.100948. 10.1016/j.jhepr.2023.100948 . hal-04264177

HAL Id: hal-04264177

<https://hal.science/hal-04264177v1>

Submitted on 30 Oct 2023

HAL is a multi-disciplinary open access archive for the deposit and dissemination of scientific research documents, whether they are published or not. The documents may come from teaching and research institutions in France or abroad, or from public or private research centers.

L'archive ouverte pluridisciplinaire **HAL**, est destinée au dépôt et à la diffusion de documents scientifiques de niveau recherche, publiés ou non, émanant des établissements d'enseignement et de recherche français ou étrangers, des laboratoires publics ou privés.



Distributed under a Creative Commons Attribution - NonCommercial 4.0 International License

1
2
3
4
5
6
7
8
9
10
11
12
13
14
15
16
17
18
19
20
21
22
23
24
25
26
27
28
29
30
31
32
33
34
35
36
37

Time-of-day-dependent variation of the human liver transcriptome and metabolome is disrupted in MASLD

Manuel Johanns¹, Joel T. Haas¹, Violetta Raverdy², Jimmy Vandel¹, Julie Chevalier-Dubois¹, Loic Guille¹, Bruno Derudas¹, Benjamin Legendre², Robert Caiazzo², Helene Verkindt², Viviane Gnemmi³, Emmanuelle Leteurtre³, Mehdi Derhourhi⁴, Amélie Bonnefond^{4,5}, Philippe Froguel^{4,5}, Jérôme Eeckhoute¹, Guillaume Lassailly⁶, Philippe Mathurin⁶, François Pattou^{2,§}, Bart Staels^{1,§}, Philippe Lefebvre^{1,§,*}

¹ Univ. Lille, Inserm, CHU Lille, Institut Pasteur de Lille, UMR1011-EGID, F-59000 Lille, France.

² Univ. Lille, Inserm, CHU Lille, Institut Pasteur de Lille, UMR1190-EGID, F-59000 Lille, France.

³ Univ. Lille, Inserm, CHU Lille, UMR 1172, Lille, France

⁴ Univ. Lille, Inserm, CHU Lille, Institut Pasteur de Lille, UMR 1283/8199-EGID, F-59000 Lille, France.

⁵ Department of Metabolism, Imperial College London; London, United Kingdom

⁶ Univ. Lille, Inserm, CHU Lille, UMR 995-LIRIC, Lille, France

§ These authors contributed equally to this work.

* Corresponding author:

Philippe Lefebvre

Inserm UMR1011, Bldg J&K

Faculté de Médecine Henri Warembourg, Pôle Recherche

Blvd du Prof Leclerc

59000, Lille, France

philippe-claude.lefebvre@inserm.fr

Tel +33.3.20974220

Keywords: Liver homeostasis/cohort/daytime rhythmicity /gene expression/metabolomic

Short title: Time-of-day-dependent rhythmicity in MASLD

Electronic word count: Abstract=222, main text=6,984

Number of figures and tables: 7/1

Use of AI in writing: none

Conflicts of interest: none

38 **Financial disclosure:** Funding sources were neither involved in the conduct of the research
39 nor in the preparation of the article. They had no role in study design, in data collection,
40 analysis and interpretation; in the writing of the report; and in the decision to submit the
41 article for publication

42

43 **Author's contributions:** Conceptualization: MJ, JTH, JV, FP, BS, PL; Software: MJ, JTH, JV, MD;
44 Validation: MJ, JTH, JV, BD, VR, JE, BS, PL; Formal analysis: MJ, JTH, JV, JE, PL; Investigation:
45 MJ, JTH, JV, BD, MD, AB; Resources: AB, PF, FP, BS, PL; Data curation: MJ, JTH, JV, BD, MD, VR,
46 PL; Writing: MJ, JTH, JV, BS, PL; Visualization: MJ, JTH, JV, PL; Supervision: BS, PL; Project
47 administration: BS, PL ; Funding acquisition: FP, BS, PL.

48

ABBREVIATIONS

ANOVA	Analysis of variance
cAMP	Cyclic adenosine monophosphate
CCGs	Core clock genes
CRN	Clinical research network
DiHOME	Dihydroxy-9-octadecenoic acid
GO	Gene ontology
GPC	Glycerophosphocholine
HFD	High fat diet
HODE	Hydroxyoctadecadienoic acid
KEGG	Kyoto encyclopedia of genes and genomes
LPA	Lysophosphatidic acid
MASLD	Metabolic dysfunction-associated steatotic liver disease
MASH	Metabolic dysfunction-associated steatohepatitis
PA	Phosphatidic acid
PNPLA3	Patatin-like phospholipase domain-containing protein 3
PPAR γ	Peroxisome proliferator-activated receptor gamma
PUFAs	Polyunsaturated fatty acids
TDG	Time-of-day-dependent genes
TDM	Time-of-day-dependent metabolites
TGF β	Transforming growth factor beta
TLR	Toll-like receptor
TNF α	Tumor necrosis factor-alpha
TTFLs	Transcriptional-translational feedback loops

51
52
53
54
55
56
57
58
59
60
61
62
63
64
65
66
67
68
69
70
71
72
73
74
75
76
77
78
79
80
81
82
83
84

ABSTRACT

Background and aims: Liver homeostasis is ensured in part by time-of-day-dependent processes, many of them being paced by the molecular circadian clock. Liver functions are compromised in metabolic dysfunction-associated steatotic liver (MASL) and metabolic dysfunction-associated steatohepatitis (MASH), and clock disruption increases susceptibility to metabolic dysfunction-associated steatotic liver disease (MASLD) progression in rodent models. We therefore investigated whether time-of-day-dependent transcriptome and metabolome are significantly altered in human steatotic and MASH livers.

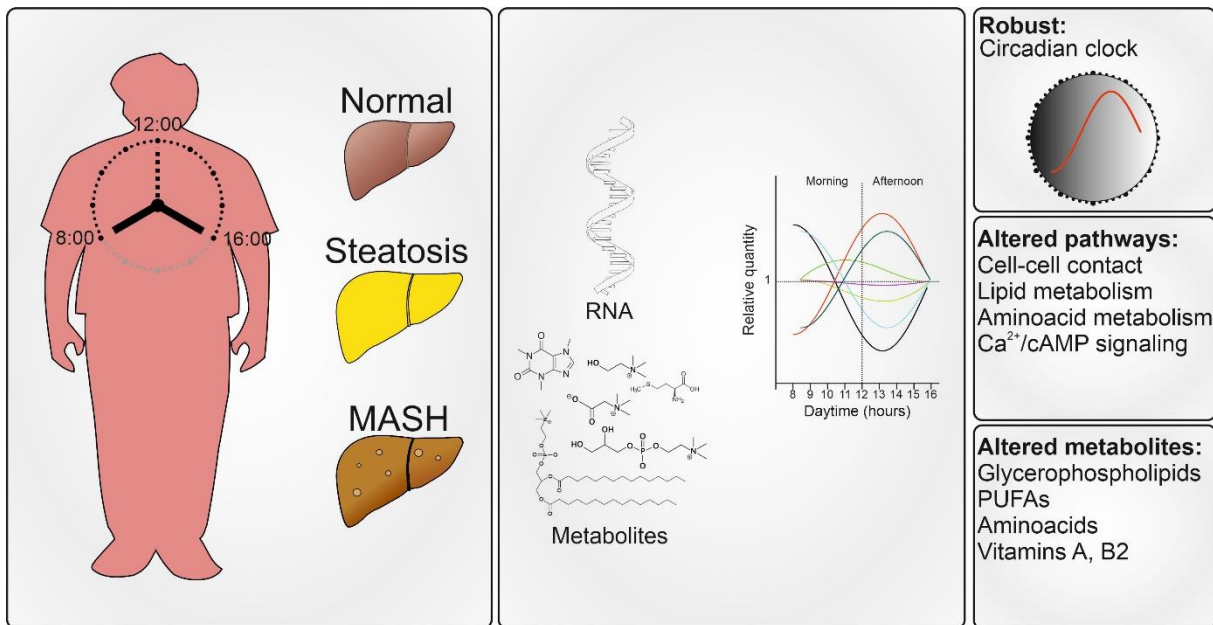
Methods: Liver biopsies, collected within an 8 hour-window from a carefully phenotyped cohort of 290 patients and histologically diagnosed to be either normal, steatotic or MASH hepatic tissues, were analyzed by RNA sequencing and unbiased metabolomic approaches. Time-of-day-dependent gene expression patterns and metabolomes were identified and compared between histologically normal, steatotic and MASH livers.

Results: We provide here a first-of-its-kind report of a daytime-resolved human liver transcriptome-metabolome and associated alterations in MASLD. Transcriptomic analysis showed a robustness of core molecular clock components in steatotic and MASH livers. It also revealed stage-specific, time-of-day-dependent alterations of hundreds of transcripts involved in cell-to-cell communication, intra-cellular signaling and metabolism. Similarly, rhythmic amino acid and lipid metabolomes were affected in pathological livers. Both TNF α and PPAR γ signaling were predicted as important contributors to altered rhythmicity.

Conclusion: MASLD progression to MASH perturbs time-of-day-dependent processes in human livers, while the differential expression of core molecular clock components is maintained.

85 **Impact and implications:** This work characterizes the rhythmic patterns of the transcriptome
 86 and metabolome in human liver. Using a cohort of in-depth phenotyped patients (n=290) with
 87 known biopsy collection time-of-day, we show that time-of-day variations observed in
 88 histologically normal livers are gradually perturbed in liver steatosis and metabolically-
 89 associated steatohepatitis. Importantly, these observations, albeit obtained on a restricted
 90 time window, bring further support to preclinical studies evidencing alterations of rhythmic
 91 patterns in diseased livers. On a practical side, this study calls for considering time-of-the-day
 92 as a critical biological variable which may significantly affect data interpretation in animal and
 93 human studies of liver diseases.

94
 95
 96
 97
 98 **Graphical abstract:**



99
 100
 101
 102
 103
 104
 105
 106
 107

109 Normal tissue homeostasis requires a precisely timed expression of genes and proteins
110 around the clock and its alignment with cycles of light/dark exposure, feeding periods and
111 physical activity. The central clock, located in the suprachiasmatic nucleus, is light-entrained
112 and connects with peripheral tissues to synchronize clock oscillators in these tissues. However,
113 peripheral tissue clocks can operate autonomously, *i.e.* independently of the central
114 hypothalamic clock. For example, the major *Zeitgeber* (“time giver”) setting the liver clock is
115 food intake/nutrient availability rather than daylight [1, 2]. Studies in nocturnal rodents of
116 molecular mechanisms controlling these circadian regulations generated a global picture
117 defining an universal molecular clock machinery [3]. This cell-autonomous circadian core clock
118 is made of 2 autoregulatory loops comprising 14 transcription factors, encoded by so-called
119 core clock genes (CCGs). Heterodimeric BMAL1 (*ARNTL*) and CLOCK (or NPAS2) transcriptional
120 activators and PER and CRY transcriptional repressors, along with the nuclear receptors RORs,
121 REV-ERB α and β constitute interlocked transcriptional-translational feedback loops (TTFLs).
122 These TTFLs define a cell-autonomous clock machinery which controls clock output genes [4],
123 in turn regulating multiple cellular functions [3].

124 Because most of primates (including humans) are diurnal, there are likely important
125 differences from rodents in circadian regulation that have yet to be explored. A limited
126 number of human time-of-day-resolved transcriptomes is available, especially for internal
127 organs. Transcriptomes from whole blood [5, 6], peripheral blood mononuclear cells [7], skin
128 [8], subcutaneous white adipose tissue [9, 10], heart montaigne [11] or skeletal muscle [12-
129 14] were analyzed for a relatively low number of subjects ($n < 30$). A gene expression study in
130 subcutaneous white adipose tissue and skin from 625 healthy volunteers allowed the
131 identification of time-of-day-regulated genes strongly enriched in CCGs [15].

132 Circadian rhythm dyssynchrony is observed in, and likely causative of, various diseases
133 such as obesity and its complications like metabolic dysfunction-associated steatotic liver
134 disease (MASLD), formerly known as non-alcoholic fatty liver disease (NAFLD). MASLD is a
135 spectrum of liver conditions characterized by hepatic steatosis which combines, upon time,
136 with varying degrees of necroinflammation and excluding excessive alcohol consumption [16].
137 Its more severe, yet generally asymptomatic form, called metabolic dysfunction-associated
138 steatohepatitis (MASH; formerly known as NASH, non-alcoholic steatohepatitis), may evolve

139 towards liver fibrosis, cirrhosis and hepatocellular carcinoma Large-scale MASLD patient
140 cohort studies reported differences in gene expression between disease stages without time-
141 of-day information [17-20]. While hepatic metabolomes and transcriptomes are deregulated
142 in rodent models of MASH and fibrosis [21, 22], whether this occurs similarly in human MASLD
143 remains unknown. A 24 hour-circadian transcriptome atlas of 64 tissues from healthy
144 baboons identified only a small set of robustly cycling genes in liver, surprisingly not including
145 CCGs [23]. Rhythmic gene expression patterns were inferred from the analysis of tissues
146 collected *post mortem* from 600 human donors. Relatively few genes (n=648), including only
147 a few CCGs, exhibited predicted time-of-day-dependent expression [24]. Thus, both ethical
148 and technical hurdles hinder the thorough investigation of time-of-day-dependent processes
149 in healthy human liver and the deregulation thereof in MASLD. Importantly, this conclusion
150 extends to the hepatic metabolome, which is clock-controlled and disturbed in various liver
151 dysfunction models [22, 25-28]. Disturbances in the hepatic chronometabolome observed in
152 rodent MASLD models have not been reported for humans so far [29].

153 Considering these knowledge gaps, we asked whether the hepatic time-of-day-
154 dependent transcriptome and metabolome are affected during MASLD progression. We
155 leveraged a large cohort of morbidly obese patients undergoing bariatric surgery from whom
156 liver biopsies were taken peri-operatively (HUL cohort, [18]). Hepatic transcriptomes and
157 metabolomes were obtained from a sub-cohort of 290 patients whose biopsies were
158 histologically identified as either normal, steatotic, or MASH livers and for which the exact
159 biopsy time-of-day was known (Figure 1A). In an original approach integrating multiple
160 statistical tests, we provide the first-ever robust analysis of time-of-day-dependent gene
161 expression and tissue metabolite abundance in human liver, as well as changes associated
162 with the different stages of MASLD.

163

164

MATERIALS and METHODS

165

166 **Liver biopsies from the HUL cohort**

167 The Hôpital Universitaire de Lille (HUL) cohort, also known as the Biological Atlas of Severe
168 Obesity (ABOS) cohort was established as from 2006 by the University Hospital of Lille, France
169 (ClinicalTrials.gov: NCT01129297) from severely and morbidly obese patients visiting the Obesity
170 Surgery Department. The study protocol conforms to the ethical guidelines of the 1975 Declaration of
171 Helsinki. All patients of the cohort fulfilled criteria for, and were willing to undergo, bariatric weight-
172 loss surgery (for details, see [18]). Written informed consent was obtained from each patient included
173 in the study. The protocol required that patients were fasting from midnight to surgery time. During
174 the surgical procedure, wedge biopsies were taken from the liver to be immediately snap-frozen and
175 the exact time of the biopsy was noted. A total of > 1,500 patients are currently included in the HUL
176 cohort, amongst whom 319 were selected to build a sub-cohort with complete clinical, biometric
177 parameters and a robust histological MASLD classification of quality-controlled biopsies eliminating all
178 intermediary MASLD stages (see [18] and Figure 1B for more details). Both transcriptomes and
179 metabolomes were obtained for these 319 patients with biopsy mass >100mg. Out of these, 290 had
180 known biopsy time-of-day, ranging from 8am to 4pm, and were included in this study. Main clinical
181 and histological characteristics are indicated in Table 1. Patient clinical data shown in Table 1 were
182 analyzed using the package “gtsummary” (v1.5.0).

183

184 **Total RNA sequencing and data processing**

185 A detailed procedure can be found in the Supplemental Information file.

186

187 **Liver metabolomics by LC-MS**

188 All tissue samples were flash frozen and maintained at –80°C until processing. Sample preparation was
189 carried out as described previously [30] at Metabolon, Inc. (Morrisville, NC, USA). A detailed procedure
190 can be found in the Supplemental Information file.

191

192 **Bioinformatic analysis**

193 **Bulk RNAseq:** All analyses were carried out using RStudio (v1.4.1106) with R (v4.1.0). Data processing
194 for differential expression as a function of time-of-day can be found in the Supplemental Information
195 file.

196

197 **Single cell RNAseq:** All analysis has been made under R (v 4.2.0). A detailed procedure for data
198 extraction and processing can be found in the Supplemental Information file.

199

200 **Enrichment analysis**

201 Time-dependent gene lists were analyzed for enrichment of Kyoto Encyclopedia of Genes and
202 Genomes (KEGG) pathways and gene ontology (GO) biological process terms using Metascape 3.5 [31]
203 with default settings (<https://metascape.org/>). A detailed procedure for data processing can be found
204 in the Supplemental Information file.

205

206 **Data visualization and illustrations**

207 Graphs were generated as *.svg files using R packages mentioned above. Data were imported in
208 CorelDraw2020 to assemble figures. Drawings in Figure 1A are from Renée Gordon, Victovoi, and
209 Mikael Häggström, M.D. and were made available to the public domain via Wikimedia Commons with
210 no restriction of use. Bubbleplots were generated in R studio using the ggplot2, plotly, reshape2, rcpp,
211 and tidyverse packages as described in [32].

212

RESULTS

Time-of-day is a major factor affecting gene expression in human liver

Human liver biopsies were collected from patients with obesity and undergoing bariatric surgery, for which the exact daytime of the liver biopsy was recorded (Figure 1A). Key clinical parameters of the 290 patients are summarized in Table 1. Based on histological features of liver biopsies (steatosis, hepatocyte ballooning, lobular inflammation), patients were grouped according to MASLD stages and labelled as histologically normal (HN), steatotic or MASH liver following the decision tree shown in Figure 1B. The proportion of men in this cohort increased with MASLD severity, rising from 16% (HN) to 38% (MASH) with an average Clinical Research Network (CRN) NAS score rising from 0 to 5, respectively. Since sex is an important biological variable in this context [18], this was considered during further analysis (see below). Patients in the steatosis and MASH groups were slightly older than those in the HN group, and expectedly had also higher insulin resistance on average.

The source of variation in gene expression levels was estimated by a multivariate analysis of variance (ANOVA) (Figure 1C). The F-ratio (ratio of the between-group variance to the within-group variance) not only confirmed sex and group (*i.e.* MASLD stage) as the main sources of variation as previously reported [18], but very interestingly identified biopsy time (AM vs. PM) as the third most significant source of variation (Figure 1C). Age had only a minor contribution to signal variation. The distribution of biopsy times (Figure 1D) revealed a daytime window of about 8 hours. Biopsies were predominantly (>60%) taken in the morning with a first peak around 9:30 AM and a second, lower peak around 2:30 PM, due to the logistical schedule of surgical interventions. There was, however, no significant difference in biopsy time distribution between histological groups (Table 1). Since exclusion of biopsies collected between 11am and 1pm did not modify the outcomes of preliminary statistical analysis, the “AM” subgroup was defined as biopsies taken before noon (12:00), the “PM” subgroup as biopsies taken after noon.

Gene expression profiles were thus compared between morning (AM) vs. afternoon (PM) samples. Differentially expressed genes were identified using DEseq2 independent of the MASLD status but correcting for sex. Transcript counts for 1,660 genes were significantly

243 different (Benjamini-Hochberg adjusted p-value <0.05) between AM or PM biopsies (Figure
244 1E). Among the 100 top hits were most of the CCGs (*PER3*, *ARNTL/BMAL1*, *NPAS2*, *NR1D1*,
245 *NR1D2*, *PER2*, *CRY1*, *PER1*), clock-related genes (*CIART*, *DBP*, *NFIL3*) (Figure 1E) as well as
246 circadian-regulated genes involved in lipid metabolism (*PPARD*, *LIPG*, *LPIN2*...). Because
247 patients were fasting from midnight irrespective of surgery time, genes implicated in hepatic
248 gluconeogenesis (*G6PC*, *PCK1*, *SGK2*...) were, as expected, higher expressed in PM samples
249 (Figure 1E and Supp. Table 1). Opposite to nocturnal rodents, genes from the negative limb of
250 the clock displayed lower expression in the afternoon (*PER3*, *NR1D1*, *NR1D2*, *CIART*...),
251 whereas genes from the positive clock limb were higher expressed in the afternoon
252 (*ARNTL/BMAL1*, *NPAS2*...)(Figure 1E). Globally, genes displaying AM vs. PM differential
253 expression were significantly enriched for the KEGG pathways “circadian rhythm”, “PPAR
254 signaling pathway”, carbohydrate and lipid metabolic pathways, as well as cellular
255 architecture and communication, among others (Figure 1F).

256 Thus an 8-hour time frame allowed the detection of significant changes in time-of-day-
257 dependent liver gene expression, with a large proportion of transcripts functionally related to
258 circadian rhythmicity.

259

260 **Time-dependent genes vary between MASLD stages**

261 We next examined whether time-of-day-dependent distributions of gene expression
262 would differ between the histological states “HN”, “steatosis” and “MASH”. In order to
263 achieve statistical power and obtain robust and exhaustive lists of time-dependent gene
264 expression over the available daytime window, we used 3 complementary statistical methods
265 analyzing different aspects of gene expression distribution (differential expression, partial
266 Spearman correlation, Kolmogorov-Smirnov test), the results of which were agglomerated by
267 a Fisher test to yield a combined p-value for each gene (Figure 2A-C and Supp. Figures 1 and
268 2). The 3 types of analyses are graphically exemplified for the core clock gene *ARNTL/BMAL1*
269 (Figure 2A-C) which served as positive control to validate our approach, as it is among the
270 most highly time-dependent genes regardless of the histological group. First DEseq2, which
271 relies on a negative binomial distribution of gene expression, was used to identify differential
272 gene expression between 2 conditions (AM vs. PM as in Figure 1) (Figure 2A). Second, partial

273 Spearman correlation was computed between *ARNTL* gene expression and daytime (Figure
274 2B). Both approaches integrated sex as a confounding factor. Third, the Kolmogorov-Smirnov
275 test was employed to determine whether AM and PM *ARNTL* expression distribution followed
276 a similar law and thus were similar in shape (Figure 2C). Finally, the Fisher combined
277 probability test or “Fisher’s method” was used as a meta-analysis method for p-value
278 combination: individual raw p-values resulting from each statistical test were agglomerated
279 into a single p-value per group (Figure 2D). The detected expression profile of *ARNTL*, of other
280 CCGs (Supp. Figure 1) and of all other transcripts (Supp. Figure 2), clearly confirmed that the
281 available time window was sufficient for robust time-of-day analysis of gene expression. A
282 total of 1,427 genes with an absolute fold change greater than 1.2 (AM vs. PM) (FDR <0.01)
283 was identified (Figure 2E). The vast majority of these time-dependent genes (TDGs) were
284 strikingly distinct when comparing the 3 patient groups. Less than 10% (132 genes) were
285 indeed common to all 3 groups (“common TDGs”) (Figure 2E) and notably included most CCGs
286 (*ARNTL*, *NR1D1/2*, *NPAS2*, *CRY1*, *PER1/2/3*, *DBP*, *CIART*)(Supp. Table 1). TDG repartition
287 outside of this core set was strongly unequal between groups, with ≈50% (558) of non-shared
288 TDGs found in HN, ≈35% (392) in steatotic and less than 15% (177) in MASH livers. Along the
289 same line, we found that AM to PM fold changes of common TDGs were, on average,
290 decreased in steatotic and even more in MASH livers when compared to HN livers (Figure 2F).
291 These differences are illustrated for a selection of TDGs with AM-PM differences either
292 decreasing (*PCAT18*, *ARMC4*, *SIK1B*) or increasing in MASH (*CYP4Z1*, *RHOBTB1*,
293 *PPIAP71*)(Figure 3A,B).

294 Common TDGs were collectively enriched for KEGG terms like “circadian rhythms” as
295 expected from the content in transcripts coding for CCGs, and for metabolic regulatory
296 pathways like the PPAR and FoxO pathways (Figure 4, Supp. Figure 3), illustrated by genes
297 such as *S1PR1*, *G6PC1*, *PCK1*, *SGK2*, *FASN*, *AQP7* and *PPARD*. TDGs unique to the HN group
298 were also enriched, albeit to a lesser extent, for pathways linked to circadian rhythm (notably
299 including *CLOCK*) as well as to fatty acid and amino acids metabolism. The most highly
300 represented pathway was “gap junctions” (Figure 4A, Supp. Figure 3), characterized by genes
301 such as *PDGFB*, *MAP2K1* and transcripts encoding for tubulins *TUBA1C/8*, *TUBB*, *TUBB1/2B*
302 (Supp. Table 1), suggesting that epithelial barrier integrity/permeability homeostasis, which is
303 known to be disturbed in MASLD [33], requires an oscillating expression of these genes in

304 healthy conditions. Genes unique to the steatosis group (Supp. Table 1) were mostly linked to
305 metabolism of lipids and fatty acids (*DGKG*, *PLA2G4B/5*, *LPIN2/3*, *ETNK2*, *ETNPPL*, *PLPP4*,
306 *FADS1/2*, *CYP2C8*, *GDPD1*, *SCD*) and also to metabolism of peptides and amino acids
307 (*DNMT3B*, *GCLM*, *SDS*, *PSAT1*, *GNMT*, *ALDOC*, *GPT2*, *CSAD*, *UPB1*)(Figure 4A, Supp. Figure 3).
308 Lastly, TDGs specific to the MASH group (Supp. Table 1) were highly enriched for signaling by
309 calcium, cAMP or neurotransmitters (*ADRB2*, *DRD1*, *GRM1*, *NTRK1*, *NTSR1*, *P2RX7*, *RYR2*,
310 *CACNA1H*, *SSTR5*, *TBXA2R*, *FFAR2*, *SUCNR1*) as well as for lipolysis (*ADRB2*, *IRS1*,
311 *PNPLA2*)(Figure 4, Supp. Figure 3). The temporal pattern of gene expression in homeostatic
312 conditions is thus strongly affected by the disease state and indicative of compromised cellular
313 communication and metabolic pathways.

314 Inferring upstream regulatory cues or altered biological processes may be achieved by
315 comparing differentially expressed gene lists to consensus gene expression patterns induced
316 by a given perturbation (Figure 4B-D). Speed2 (Signaling Pathway Enrichment using
317 Experimental Datasets [34]) analysis allows probing gene lists against ranked gene signatures
318 for 16 signaling pathways, with the aim of identifying upstream signaling mediators. Ranked
319 signatures suggested that cues in homeostatic (HN) conditions could be TGF β , TNF α , oxidative
320 stress, TLR and estrogen (Figure 4B). In steatosis and MASH conditions, this pattern shifted
321 towards a more limited signaling pathway panel with similar statistical significance, which
322 included either TLR and VEGF (steatosis) or TNF α and TLR (MASH)(Figure 4C and 4D
323 respectively). Although causative links cannot be proven, this data could reflect a loss of
324 physiological rhythmic function(s) in steatotic and MASH livers, which in turn gain rhythmic
325 functions associated to pathogenic immune and proliferative stimuli and responses.

326

327 **MASLD stages correlates with time-of-day changes in liver metabolites**

328 Our results suggested that metabolic pathways are altered in a time-of-day-dependent
329 manner as MASLD progresses, with an enrichment in amino acid- and lipid metabolism-
330 regulating genes (Supp. Figure 3). Therefore, an unbiased tissue metabolomic study by LC-MS
331 was performed on the same 290 liver samples. Similar to the gene expression analysis, a
332 global approach was initially employed to evaluate overall time-of-day dependence of tissue
333 metabolite levels regardless of the MASLD status. This global analysis identified \approx 220
334 metabolites whose amounts were significantly different in AM and PM biopsies (DEseq2

335 corrected for sex, FDR<0.1) (Figure 5A, Supp. Table 2). Visual inspection of the volcano plot
336 highlighted intermediates of lipid β -oxidation (carnitine derivatives), amino acids (kynurenate,
337 oxo-arginine...) as differentially detected in AM vs. PM livers (Figure 5A). It also confirmed the
338 more marked fasting status of "PM" patients exhibiting an increased hepatic content in 3-
339 hydroxybutyrate (BHBA). A biological term enrichment analysis confirmed that the majority of
340 the identified metabolites belonged to amino acid, lipid and fatty acid metabolic pathways
341 (Figure 5B).

342 To highlight a possible time-of-day differential representation of metabolites between
343 MASLD groups, we again combined the 3 statistical approaches as described for gene
344 expression analysis (DEseq2, Spearman correlation, Kolmogorov-Smirnov test) followed by
345 Fisher's agglomeration for a robust identification of time-dependent metabolites (TDMs)
346 (Figure 5C). A total of 251 TDMs were identified using this method (combined FDR<0.1), out
347 of which only 14 (6%) were common to all 3 MASLD groups (Figure 6A, 6B). These common
348 TDMs included amino acids such as proline and threonine, several fatty acids and the ketone
349 body component β -hydroxybutyrate (Figure 6B and Supp. Figure 4A-F). KEGG metabolic
350 pathway enrichment analysis revealed that these common TDMs were most significantly
351 associated to metabolism of amino acids (arginine, proline, threonine)(Figure 6B and Supp.
352 Figure 4A-C). In agreement with the identification of the PPAR pathway based on gene
353 expression patterns (Figure 4) and the detection of 3-hydroxybutyrate (Supp. Figure 4D),
354 synthesis of ketone bodies was also identified as a relevant term (Figure 6B),

355 Among the 197 stage-specific TDMs, 31% were specific to HN, 47% to steatosis and
356 20% to MASH (Figure 6A and Supp. Table 2). TDMs specific to HN livers, and thus lost at the
357 steatosis and MASH stages, were mainly associated to metabolism of sphingolipids (Figure 6C
358 and Supp. Table 2) such as CDP-choline and sphinganine (Supp. Figure 4G, H).
359 Glycerophosphoethanolamines, glycerophosphocholines as well as derivatives of cholesterol,
360 amino acids and pyrimidine were also identified as time-dependent in normal livers (Supp.
361 Table 2 and Supp. Figure 4I-L).

362 A similar enrichment analysis identified amino acid metabolic pathways (branched-
363 chain, sulfur-containing, arginine, taurine) (Figure 6D, Supp. Figure 5A, B and Supp. Table 2) as
364 time-dependent in steatotic livers. Visual inspection of steatosis TDMs also identified a
365 carnitine precursor (N6,N6,N6 trimethyl-lysine, Supp Figure 5C) and derivatives (Supp. Table

366 2 and Supp. Figure 5D, E) which could reflect an altered fatty acid oxidation activity. Finally,
367 MASH-specific TDMs were enriched mainly for vitamin, glycan and
368 glycosylphosphatidylinositol (GPI) metabolic intermediates (Figure 6E, Supp. Figure 5 and
369 Supp. Table 2).

370 Taken together, these analyses highlight the disruption during MASLD progression of
371 time-of-day-dependent bioactive phospholipid metabolism and of amino acid
372 biotransformation pathways. Intriguingly, PPAR γ ligands of the linoleic acid class (9,10
373 DiHOME [35] and 9- and 13-HODE [36]) displayed a differential abundance in AM vs. PM
374 steatotic and MASH livers, with estimated concentrations in the 10-100 μ M range which are
375 sufficient to activate PPAR γ (Supp. Figure 5F, J).

376

377 **Integrative analysis of time-dependent genes and metabolites.**

378 We next performed an integrative analysis of the transcriptomic and metabolomic data
379 at the pathway level using the KEGG database. This analysis combined TDGs and TDMs specific
380 to either HN or MASH stages and common TDGs and TDMs, irrespective of their relative time-
381 of-day direction of change, to identify associated transcriptomic and metabolomic conditions
382 operating in normal and MASH livers (Figure 7A). TDGs and TDMs characterizing the HN stage
383 were enriched for metabolic pathways related to lipid and amino acid metabolism, while most
384 of them were not detected at the MASH stage, or with a decreased significance [arginine (Arg)
385 and proline (Pro) metabolism, glycerophospholipid metabolism]. Linoleic metabolism was
386 associated to the MASH stage (Figure 7B, C). HN-or MASH-enriched pathways
387 (glycerophospholipid and linoleic pathways, respectively) were further detailed for daytime
388 variation of associated TDGs and TDMs. The glycerophospholipid pathway was characterized
389 by an increased abundance in AM livers of 3 out of 4 detected diacylglycerol (DAG) species
390 specifically at the HN stage. Glycerophosphocholine (GPC) intermediates (CDP-choline, GPC)
391 displayed stage-specific time-of-day variations that were not correlated to the occurrence of
392 glycerophospholipid species (X-GPC) (Figure 7D). Higher abundance of DAG species in the
393 morning did not correlate with HN TDG expression changes in transcripts encoding enzymes
394 involved in this metabolic pathway, with the exception of the patatin-like phospholipase
395 domain-containing protein 3-encoding gene (*PNPLA3*). *PNPLA3*/adiponutrin has

396 acyltransferase activity, increasing the formation of phosphatidic acid (PA) from
397 lysophosphatidic acid (LPA), which may lead to more DAG synthesis. It might also reflect
398 PNPLA3 hydrolytic activity on triacylglycerol molecules, favoring DAG accumulation. Along the
399 same line, we compiled TDG and TDM data related to linoleic acid metabolism (Figure 7E). The
400 increased abundance of the PPAR γ ligands 9- and 13-HODE in the afternoon at the MASH stage
401 was mirrored by the gene expression of *ALOX15*, a dioxygenase catalyzing the synthesis of
402 these 2 hydroxyoctadecadienoic acids which was higher in the morning. A similar lack of
403 correlation was observed between 9,10-DiHOME hepatic content and the expression of the
404 linoleic acid-converting *CYP2C8* at the steatosis stage. These results suggest that time-
405 dependent metabolite variation in these pathways is delayed with respect to gene regulation,
406 and/or controlled by post-transcriptional processes.

407 Of note, mapping of human transcript expression to liver cell types using a reference
408 single cell RNAseq dataset [37] suggested that the identified enzymatic pathways may follow
409 a cell-specific expression pattern. They appear as mainly restricted, but not limited to,
410 hepatocytes. As an example, *ALOX15* is detected in dendritic cells, whereas *ALOX5* is also
411 detected in monocytes, neutrophils and basophils (Supp. Figure 6). Therefore time-
412 dependent metabolite variation may occur in either identical or distinct cell types, reflecting
413 a functional compartmentalization. Yet these observations confirmed the presence of time-of
414 day variation in hepatic gene expression and metabolome, and identified several new
415 oscillating metabolites at the MASH stage (Figure 7 and Supp. Table 2).

416

417

DISCUSSION

418 Chronobiological studies require multiple replicates at 2h-intervals over a total period
419 of 24 or even 48 hours, within a controlled environment including timed exposure to light and
420 food. These conditions are not achievable in human studies, precluding the analysis of cyclic
421 processes and particularly in internal organs [38]. While human circadian rhythms are
422 appreciated by genome-wide association study studies and the phenotypic manifestation of
423 disturbed cyclic processes such as sleep, light exposure and eating patterns [39], their study
424 in healthy or pathological conditions is indeed hindered by ethical and technical constraints.
425 Despite controlled experimental setup with regard to sleep behavior and food intake in
426 previous studies [5-14], a limited number of samples of mostly healthy individuals were
427 collected, thereby limiting data interpretation due to high inter-sample variability.

428 Here we reveal the first ever time-of-day-resolved human liver transcriptome with
429 associated liver tissue metabolites using a 290-patient cohort. Although the available time
430 window of liver biopsies was only about 8 hours, this temporal window was sufficient to
431 robustly identify TDGs and TDMs. Time-dependency of genes and metabolites was distinct
432 between histologically-defined MASLD groups. However, a small proportion of genes was
433 identified as time-dependent in all three patient groups and included CCGs, indicating that the
434 molecular lock is rather robust in pathological conditions. In contrast, the alignment of
435 rhythmic biological processes such as intercellular communication (gap junctions) and
436 metabolic regulations is disrupted upon MASLD progression. Interestingly, none of the
437 detected TDGs in MASH patients belonged to the human and mouse core set of
438 MASH/fibrosis-associated genes [20], underlining the need for considering time as an
439 important biological variable. Interestingly, the number of stage-specific TDGs (Figure 2E)
440 decreases from the HN to the MASH stage, and concomitantly enriched pathways lessen
441 (Supp. Figure 3), hinting at a loss of functional adaptability/(metabolic) flexibility. In high fat
442 diet (HFD)-fed mice, transcripts gaining rhythmicity when compared to chow diet-fed mice are
443 strongly enriched for glycerophospholipid metabolism [22], similarly to steatotic patients (Supp.
444 Figure 3), indicating convergent mechanisms for liver adaptation to dietary imbalance as often
445 occurring in MASLD. At the cellular level, Ca^{2+} fluxes are submitted to ultradian variations and
446 coupled to metabolic regulations [40], and mishandled intracellular Ca^{2+} stores in MASH can
447 significantly impact parenchymal and non-parenchymal liver cellular functions [41]. A number

448 of genes encoding for Ca²⁺ channel components or involved in intracellular Ca²⁺ signaling
449 (*PKD1L1*, *TRPC1*, *P2RX7*, *FFAR2*, *ADRB2*, *CACNA1H*, *GRM1*, *NTRK1*) exhibited differential AM vs.
450 PM expression specifically in MASH livers. Thus, in addition to the lipid-induced dysfunctional
451 ER Ca²⁺ transport [42], *de novo* oscillation of the calcium handling process accompanies
452 progression to MASH. *CLOCK* gene deletion affected metabolite oscillations in mouse liver
453 [25] and we detected a time-of-day differential expression of *CLOCK* exclusively in HN livers,
454 which display a more diverse metabolic activity than MASH livers (Figure 7B). While hinting
455 at a possible role of (the loss of) *CLOCK*, the examination of individual metabolites
456 nevertheless showed little overlap between mouse *CLOCK*-dependent metabolites and HN-
457 specific metabolites. This lack of clear concordance can be explained by species-specific
458 mechanisms, distinct effects of gene deletion vs. loss of time-dependent expression and/or
459 technical bias.

460 While examining the coherence between MASLD state-specific liver transcriptomes
461 and metabolomes, we observed little correlation between enzyme-encoding genes and
462 metabolite abundance. This disconnection is not unprecedented and was also observed in a
463 highly standardized mouse study which minimizes the variability typically observed in human
464 samples [22]. The narrow time window of our study may explain in part this lack of correlation
465 as transcripts are likely to precede metabolite production, hence affecting our statistical
466 approach for the PM sub-cohort. It may also indicate significant time-of-day-dependent
467 translational control [43] as well as post-translational modifications regulating enzyme activity
468 which are not captured by our analysis.

469 Finally, another point of convergence between our and mouse studies is the
470 differential abundance of linoleic acid derivatives and PPAR γ ligands 9,10-DiHOME, 9-HODE
471 and 13-HODE in steatotic and MASH livers, respectively. The PPAR γ -encoding gene
472 *NR1C3/PPARG* itself did not display significant oscillatory expression in human liver,
473 contrasting with HFD mouse livers [22]. Whether estimated released concentrations of these
474 compounds are indeed sufficient to differentially activate human liver PPAR γ , which is mostly
475 expressed in endothelial cells, hepatocytes and macrophages (Supp. Figure 6) and have a
476 causative role in hepatic transcriptional reprogramming requires further in-depth investigation.

477 On the one hand, it is remarkable that many of the biological processes and pathways
478 shown to be affected by MASLD in other studies, identified on the basis of changes in gene

479 expression or metabolite abundance levels regardless of time, also display altered time-
480 dependent expression profiles in our study. On the other hand, we identified many novel
481 potential links between genes with deregulated timed expression and MASLD pathogenesis,
482 which were not previously considered by standard analyses. It is probably the combination of
483 both types of deregulations that underlies the deeply disturbed liver functions once MASH is
484 declared. Conversely, some of the changes detected when time-of-day information is absent
485 or ignored may turn out to be artefacts, as time-of-day as a biological variable might not be
486 equilibrated between groups.

487 Considering that the time-of-day dependence of transcript/protein/metabolite
488 measurements was previously neglected or ignored in nearly all human MASLD studies, our
489 findings here reveal a significant impact of time-of-day on many relevant pathogenic
490 processes. As such, differences found between sample groups in cohort studies might reflect
491 a previously under-appreciated bias in sampling time between groups. Further investigation
492 is needed in this regard, particularly when studying human material. In any case, a new
493 generality should be that sampling daytimes (or *Zeitgeber* times) must be carefully recorded
494 and included in post-hoc analyses whenever possible.

495

496 **Strengths and limitations of the study.**

497 This study has both strengths and limitations. This first-of-its-kind study revealed time-
498 of-day transcriptomic and metabolomic alterations in human livers as a function of the
499 histologically-proven MASLD stage. It used a large cohort allowing both the selection of
500 biopsies to adequately encompass healthy control, steatosis and MASH cases and robust
501 statistical analysis. There is however a number of limitations, inherent to the observational
502 nature of the study. The narrow time window for biopsies collection (8 hours) precludes the
503 assessment of a 24h diurnal rhythmicity, hence of the integrity of the molecular clock. The
504 unavoidable difference in fasting duration could also be a confounding factor.

505 Our bulk RNA sequencing approach allowed a full coverage of the transcriptome, but
506 precluded the identification of liver cell types expressing TDGs. We thus calculated a cell
507 specificity index of TDGs in human resident parenchymal (PC, hepatocytes) and non-
508 parenchymal (NPC) CD45⁻ cells. The tau (τ) index, calculated by a robust and simple method

509 to assess cell-type specificity, was used as a metrics [44]. Using a reference single cell-RNA
510 sequencing dataset for human livers collected at unknown times [37], τ could be
511 calculated for 584 transcripts out of the 1,481 identified TDGs (Supp. Table 1). Using this
512 metric, only 51 genes displayed a cell type-restricted expression pattern in CD45⁻ cells
513 ($\tau > 0.85$), which was not limited to hepatocytes (Supp. Figure 7). The remaining 533 transcripts
514 including CCGs could be mapped to 2 or more cell types. Of note, 15 out of the 51 cell-
515 restricted transcripts were mostly expressed in dendritic or Kupffer cells (Supp. Figure 6).

516 Taken together, our bulk RNAseq approach detected a high number of TDGs than
517 previous efforts, including many pathways never previously reported as being time-
518 dependent. This resource will serve as an important basis for further investigations
519 considering also the cell-type specificity in time-of-day gene expression variation in human
520 MASLD.

521

522

ACKNOWLEDGMENTS

523 This work was supported by ANR (RHU PreciNASH 16-RHUS-0006, EGID ANR-10-LABX-0046
524 and DeCodeNASH ANR-20-CE14-0034). MJ was supported by Wallonie-Bruxelles International
525 (WBI, Belgium, ref. SUB/2020/479801) and from European Association for the Study of the
526 Liver (EASL, Sheila Sherlock fellowship). JTH and AB hold a European Research Council (ERC)
527 grant (StG, Metabo3DC, contract number 101042759; CoG, OpiO, contract number
528 101043671 respectively). PL's and BS's teams are supported by Fondation pour la Recherche
529 Médicale (Equipes labellisées FRM EQU202203014645 and FRM EQU202203014650
530 respectively).

531

532

DATA AVAILABILITY

533 Further information and requests for resources and data sets should be directed to and
534 will be fulfilled by the corresponding author. Data exploration of the HUL cohort is still
535 ongoing and restrictions apply to clinical data availability.

536

538 **Author names in bold designate shared co-first authorship.**

- 539 [1] Li H, Zhang S, Zhang W, Chen S, Rabearivony A, Shi Y, et al. Endogenous circadian time genes
540 expressions in the liver of mice under constant darkness. *BMC Genomics* 2020;21:224.
- 541 [2] Chaix A, Lin T, Le HD, Chang MW, Panda S. Time-Restricted Feeding Prevents Obesity and
542 Metabolic Syndrome in Mice Lacking a Circadian Clock. *Cell Metab* 2019;29:303-319.
- 543 [3] Sato T, Sassone-Corsi P. Nutrition, metabolism, and epigenetics: pathways of circadian
544 reprogramming. *EMBO Rep* 2022;23:e52412.
- 545 [4] Takahashi JS. Transcriptional architecture of the mammalian circadian clock. *Nat Rev Genet*
546 2017;18:164-179.
- 547 [5] **Archer SN, Laing EE**, Möller-Levet CS, van der Veen DR, Bucca G, Lazar AS, et al. Mistimed sleep
548 disrupts circadian regulation of the human transcriptome. *Proc Natl Acad Sci U S A* 2014;111:E682-691.
- 549 [6] **Möller-Levet CS, Archer SN**, Bucca G, Laing EE, Slak A, Kabiljo R, et al. Effects of insufficient
550 sleep on circadian rhythmicity and expression amplitude of the human blood transcriptome. *Proc Natl*
551 *Acad Sci U S A* 2013;110:E1132-1141.
- 552 [7] Kervezee L, Cuesta M, Cermakian N, Boivin DB. The phase-shifting effect of bright light
553 exposure on circadian rhythmicity in the human transcriptome. *J Biol Rhythms* 2019;34:84-97.
- 554 [8] Wu G, Ruben MD, Schmidt RE, Francey LJ, Smith DF, Anafi RC, et al. Population-level rhythms
555 in human skin with implications for circadian medicine. *Proc Natl Acad Sci U S A* 2018;115:12313-
556 12318.
- 557 [9] Christou S, Wehrens SMT, Isherwood C, Möller-Levet CS, Wu H, Revell VL, et al. Circadian
558 regulation in human white adipose tissue revealed by transcriptome and metabolic network analysis.
559 *Sci Rep* 2019;9:2641.
- 560 [10] Zhao L, Hutchison AT, Liu B, Wittert GA, Thompson CH, Nguyen L, et al. Time-restricted eating
561 alters the 24-hour profile of adipose tissue transcriptome in men with obesity. *Obesity (Silver Spring)*
562 2023;31 Suppl 1:63-74.
- 563 [11] Montaigne D, Marechal X, Modine T, Coisne A, Mouton S, Fayad G, et al. Daytime variation of
564 perioperative myocardial injury in cardiac surgery and its prevention by Rev-Erbalpha antagonism: a
565 single-centre propensity-matched cohort study and a randomised study. *Lancet* 2018;391:59-69.
- 566 [12] **Wefers J, van Moorsel D, Hansen J**, Connell NJ, Havekes B, Hoeks J, et al. Circadian
567 misalignment induces fatty acid metabolism gene profiles and compromises insulin sensitivity in
568 human skeletal muscle. *Proc Natl Acad Sci U S A* 2018;115:7789-7794.
- 569 [13] Perrin L, Loizides-Mangold U, Chanon S, Gobet C, Hulo N, Isenegger L, et al. Transcriptomic
570 analyses reveal rhythmic and CLOCK-driven pathways in human skeletal muscle. *Elife* 2018;7.
- 571 [14] van Moorsel D, Hansen J, Havekes B, Scheer FA, Jorgensen JA, Hoeks J, et al. Demonstration of
572 a day-night rhythm in human skeletal muscle oxidative capacity. *Mol Metab* 2016;5:635-645.
- 573 [15] Couto Alves A, Glastonbury CA, El-Sayed Moustafa JS, Small KS. Fasting and time of day
574 independently modulate circadian rhythm relevant gene expression in adipose and skin tissue. *BMC*
575 *Genomics* 2018;19:659.
- 576 [16] Rinella ME, Lazarus JV, Ratzliff V, Francque SM, Sanyal AJ, Kanwal F, et al. A multi-society Delphi
577 consensus statement on new fatty liver disease nomenclature. *J Hepatol* 2023, doi:
578 10.1097/HEP.0000000000000520.
- 579 [17] Govaere O, Cockell S, Tiniakos D, Queen R, Younes R, Vacca M, et al. Transcriptomic profiling
580 across the nonalcoholic fatty liver disease spectrum reveals gene signatures for steatohepatitis and
581 fibrosis. *Sci Transl Med* 2020;12:eaba4448.
- 582 [18] Vandel J, Dubois-Chevalier J, Gheeraert C, Derudas B, Raverdy V, Thuillier D, et al. Hepatic
583 Molecular Signatures Highlight the Sexual Dimorphism of Nonalcoholic Steatohepatitis (NASH).
584 *Hepatology* 2021;73:920-936.

585 [19] **Haas JT, Vonghia L, Mogilenko DA**, Verrijken A, Molendi-Coste O, Fleury S, et al.
586 Transcriptional Network Analysis Implicates Altered Hepatic Immune Function in NASH development
587 and resolution. *Nature metabolism* 2019;1:604-614.

588 [20] Lefebvre P, Lalloyer F, Bauge E, Pawlak M, Gheeraert C, Dehondt H, et al. Interspecies NASH
589 disease activity whole-genome profiling identifies a fibrogenic role of PPARalpha-regulated
590 dermatopontin. *JCI Insight* 2017;2:e92264.

591 [21] Chen P, Kakan X, Zhang J. Altered circadian rhythm of the clock genes in fibrotic livers induced
592 by carbon tetrachloride. *FEBS Lett* 2010;584:1597-1601.

593 [22] Eckel-Mahan KL, Patel VR, de Mateo S, Orozco-Solis R, Ceglia NJ, Sahar S, et al. Reprogramming
594 of the circadian clock by nutritional challenge. *Cell* 2013;155:1464-1478.

595 [23] Mure LS, Le HD, Benegiamo G, Chang MW, Rios L, Jillani N, et al. Diurnal transcriptome atlas of
596 a primate across major neural and peripheral tissues. *Science* 2018;359:eao0318.

597 [24] Ruben MD, Wu G, Smith DF, Schmidt RE, Francey LJ, Lee YY, et al. A database of tissue-specific
598 rhythmically expressed human genes has potential applications in circadian medicine. *Sci Transl Med*
599 2018;10:eaat8806.

600 [25] Eckel-Mahan KL, Patel VR, Mohney RP, Vignola KS, Baldi P, Sassone-Corsi P. Coordination of
601 the transcriptome and metabolome by the circadian clock. *Proc Natl Acad Sci U S A* 2012;109:5541-
602 5546.

603 [26] Abbondante S, Eckel-Mahan KL, Ceglia NJ, Baldi P, Sassone-Corsi P. Comparative Circadian
604 Metabolomics Reveal Differential Effects of Nutritional Challenge in the Serum and Liver. *J Biol Chem*
605 2016;291:2812-2828.

606 [27] Fujisawa K, Takami T, Matsumoto T, Yamamoto N, Sakaida I. Profiling of the circadian
607 metabolome in thioacetamide-induced liver cirrhosis in mice. *Hepato Comm* 2017;1:704-718.

608 [28] Kettner NM, Voicu H, Finegold MJ, Coarfa C, Sreekumar A, Putluri N, et al. Circadian
609 Homeostasis of Liver Metabolism Suppresses Hepatocarcinogenesis. *Cancer Cell* 2016;30:909-924.

610 [29] Malik DM, Paschos GK, Sehgal A, Weljie AM. Circadian and Sleep Metabolomics Across Species.
611 *J Mol Biol* 2020;432:3578-3610.

612 [30] Evans AM, DeHaven CD, Barrett T, Mitchell M, Milgram E. Integrated, nontargeted ultrahigh
613 performance liquid chromatography/electrospray ionization tandem mass spectrometry platform for
614 the identification and relative quantification of the small-molecule complement of biological systems.
615 *Analytical chemistry* 2009;81:6656-6667.

616 [31] **Tripathi S, Pohl MO**, Zhou Y, Rodriguez-Frandsen A, Wang G, Stein DA, et al. Meta- and
617 Orthogonal Integration of Influenza "OMICS" Data Defines a Role for UBR4 in Virus Budding. *Cell Host*
618 *Microbe* 2015;18:723-735.

619 [32] Zummo FP, Berthier A, Gheeraert C, Vinod M, Bobowski-Gerard M, Molendi-Coste O, et al. A
620 time- and space-resolved nuclear receptor atlas in mouse liver. *J Mol Endocrinol* 2023;71:e230017.

621 [33] Pradhan-Sundd T, Vats R, Russell JO, Singh S, Michael AA, Molina L, et al. Dysregulated bile
622 transporters and Impaired tight junctions during chronic liver injury in mice. *Gastroenterology*
623 2018;155:1218-1232.

624 [34] **Rydenfelt M, Klinger B**, Klunemann M, Bluthgen N. SPEED2: inferring upstream pathway
625 activity from differential gene expression. *Nucleic Acids Res* 2020;48:W307-W312.

626 [35] Lecka-Czernik B, Moerman EJ, Grant DF, Lehmann JM, Manolagas SC, Jilka RL. Divergent effects
627 of selective peroxisome proliferator-activated receptor-gamma 2 ligands on adipocyte versus
628 osteoblast differentiation. *Endocrinology* 2002;143:2376-2384.

629 [36] Nagy L, Tontonoz P, Alvarez JG, Chen H, Evans RM. Oxidized LDL regulates macrophage gene
630 expression through ligand activation of PPARgamma. *Cell* 1998;93:229-240.

631 [37] Williams M, Bonnardel J, Haest B, Vanderborcht B, Wagner C, Remmerie A, et al. Spatial
632 proteogenomics reveals distinct and evolutionarily conserved hepatic macrophage niches. *Cell*
633 2022;185:379-396.

634 [38] Klerman EB, Brager A, Carskadon MA, Depner CM, Foster R, Goel N, et al. Keeping an eye on
635 circadian time in clinical research and medicine. *Clin Transl Med* 2022;12:e1131.

636 [39] Gentry NW, Ashbrook LH, Fu YH, Ptacek LJ. Human circadian variations. *J Clin Invest* 2021;131.

- 637 [40] Yang S, Yamazaki S, Cox KH, Huang YL, Miller EW, Takahashi JS. Coupling-dependent metabolic
638 ultradian rhythms in confluent cells. *Proc Natl Acad Sci U S A* 2022;119:e2211142119.
- 639 [41] Oliva-Vilarnau N, Hankeova S, Vorrink SU, Mkrtchian S, Andersson ER, Lauschke VM. Calcium
640 Signaling in Liver Injury and Regeneration. *Front Med (Lausanne)* 2018;5:192.
- 641 [42] Arruda AP, Hotamisligil GS. Calcium Homeostasis and Organelle Function in the Pathogenesis
642 of Obesity and Diabetes. *Cell Metab* 2015;22:381-397.
- 643 [43] Castelo-Szekely V, Gatfield D. Emerging Roles of Translational Control in Circadian
644 Timekeeping. *J Mol Biol* 2020;432:3483-3497.
- 645 [44] Kryuchkova-Mostacci N, Robinson-Rechavi M. A benchmark of gene expression tissue-
646 specificity metrics. *Brief Bioinform* 2017;18:205-214.

647

648

Figure legends

649

650 **Figure 1: Timed liver biopsies from a large cohort of humans with obesity.** (A) Overall
651 experimental strategy. (B) Decision tree to stratify the HUL sub-cohort. “HN” (histologically
652 normal), “steatosis” (benign steatosis only) or “MASH” (steatosis+inflammation). (C) Inter-
653 sample variation in gene expression. ANOVA was used to reveal the main sources of overall
654 inter-sample variation. (D) Biopsy daytime distribution. (E) Gene expression analysis. A
655 volcano plot was generated by comparing gene expression using DEseq2 from samples
656 collected in the morning (AM) or in the afternoon (PM) regardless of the pathological state. X
657 axis: \log_2 (fold change), Y axis: $-\log_{10}$ (p-values). (F) KEGG pathway enrichment analysis.
658 Biological term enrichment was carried out using the 1,660 genes whose expression was
659 significantly different as determined in (E) ($FC > 1.2$, $FDR < 0.05$). (E, F): font size was adjusted
660 for clarity purpose.

661

662 **Figure 2: A multi-test method identifies time-of-day-dependent genes.** *BMAL1/ARNTL*
663 expression as a function of time and of the liver histological grade (A-C). (A) A violin plot is
664 shown to illustrate DEseq2 results to compare AM vs. PM expression and correcting for sex as
665 confounding factor. (B) A dot plot with linear tendency lines is shown to illustrate partial
666 Spearman correlation analysis between gene expression and biopsy daytime. (C) A density
667 plot is shown to illustrate the output of the Kolmogorov-Smirnov test for comparison of AM
668 or PM gene expression distributions. (D) Fisher’s agglomeration method. Frequency
669 histograms of uncorrected Fisher p-values are shown for each group and the first (colored)
670 bar of each group histogram indicates genes with $p < 0.05$. (E) TDG distribution within
671 histological groups. A Venn diagram shows the unequal distribution of 1,427 TDGs ($FC > 1.2$,
672 $FDR < 0.01$) amongst groups. Numbers indicate the numbers of identified transcripts. (F) Gene
673 expression variation of 132 “common TDGs”. CCGs and other transcripts are indicated. *
674 indicates $p < 0.05$ using ANOVA and Fisher’s LSD post-hoc test.

675

676 **Figure 3: Example distributions of time-dependent genes (TDGs) altered in MASH.** (A) Violin
677 plots showing AM vs PM gene expression variations for representative TDGs losing their time-
678 dependency in MASH. (B) Violin plots showing AM vs PM gene expression variations for
679 representative TDGs gaining time-dependency in MASH. Statistical tests were Kruskal-Wallis
680 tests followed by unpaired Wilcoxon post-hoc test for AM-PM comparisons in each group
681 (* $p < 0.05$, ** $p < 0.01$, *** $p < 0.005$, ****, $p < 0.001$). VST: variance-stabilizing transformation.

682

683 **Figure 4: Term enrichment analysis of time-dependent genes (TDGs) and upstream**
684 **regulatory pathway prediction.** (A) Biological term enrichment analysis. TDGs identified in
685 Figure 2 were enriched for gene ontology (GO) terms related to biological processes (BP) using
686 Metascape. Significantly enriched GO-BP clusters were manually collapsed for visualization
687 purpose and top hits are indicated. **(B-D):** Pathway activity ranking. Speed2 TDGs enrichment
688 for pathway signature genes. Each pathway is represented as a bar showing the mean rank of
689 the query list. The “bar code” plot shows the distribution of genes from the query list in the
690 ranked reference signatures.

691

692 **Figure 5: Identification of time-dependent liver metabolites measured by LC-MS.** (A) Volcano
693 plot of metabolite time-of-day-dependent differential abundance in liver. Fold-changes
694 values and corresponding p-values obtained using DEseq2 considering sex as confounding
695 factor. (B) Enrichment of KEGG metabolic pathways. A biological term enrichment against the
696 KEGG database was run using the differentially detected metabolites (TDM) identified in (A)
697 (DEseq2 adjusted p-value < 0.1). (C) P-value agglomeration by Fisher’s method. Similar as gene
698 expression analysis (see Figure 2), p-value agglomeration from three separate statistical tests
699 (DEseq2, partial Spearman correlation, Kolmogorov-Smirnov) was carried out using Fisher’s
700 method and identified TDMs within each group. The resulting uncorrected Fisher p-values are
701 shown as frequency histograms and the first (colored) bar of each group histogram indicates
702 metabolites with $p < 0.1$.

703

704 **Figure 6: Distribution and characterization of time-dependent liver metabolites (TDMs).**
705 After correction for multiple testing, 238 metabolites with a Fisher FDR < 0.1 were considered

706 as robustly time-dependent. (A) Distribution of TDMs among liver histological groups. (B-E)
707 KEGG metabolic pathway enrichment of common (central intersection) or group-specific
708 TDMs using the online metabolomics analysis platform MetaboAnalyst.

709

710 **Figure 7: Integrative analysis of time-dependent genes (TDGs) and metabolites (TDMs).** (A)

711 Analysis strategy outline. Common and HN- or MASH-specific TDGs and TDMs were analyzed
712 associatively for enrichment of KEGG metabolic pathways using the online metabolomics
713 analysis platform MetaboAnalyst, revealing potential links between metabolic pathways as
714 defined by time-dependent gene expression patterns and metabolomic profiling (B, C).
715 Reconstitution (partial) of metabolic pathways displaying time of the day-dependency in the
716 HN (D) or MASH (E) group. LPA: lysophosphatidic acid, PA: phosphatidic acid, DAG:
717 diacylglycerol, CDP-choline: cytidine-diphosphate-choline, PC: phosphatidylcholine, GPC
718 glycerophosphatidylcholine, X-GPC: acyl-conjugated GPC, 9-HpODE: 9-hydroperoxy
719 octadecadienoic acid, 13-HpODE: 9-hydroperoxy octadecadienoic acid, 9-HODE: 9-
720 Hydroxyoctadecadienoic acid, 13-HODE: 13-Hydroxyoctadecadienoic acid, 12(13)-EpOME:
721 12(13)-epoxy-9Z-octadecenoic acid, 9,10-EpOME: 9(10)-epoxy-12Z-octadecenoic acid, 12,13-
722 DiHOME: 12,13-dihydroxy-9-octadecenoic acid, 9,10-DiHOME: 9,10-dihydroxy-9-
723 octadecenoic acid.

724

725 **Table 1: Biometric and biochemical parameters of the HUL sub cohort.** The main biometric,
726 biochemical and liver histological features of selected patients are indicated. F: women, M:
727 men; BMI: body mass index; NAS: NAFLD/MASLD Activity Score; HOMA-IR: Homeostatic
728 Model Assessment for Insulin Resistance; AM: ante meridiem, PM: post meridiem. Continuous
729 values are expressed as mean \pm SD. Inter-group comparisons were performed using the
730 unpaired Wilcoxon test for continuous variables (age, BMI, HOMA-IR) and Fisher's exact test
731 for the remaining categorical variables.

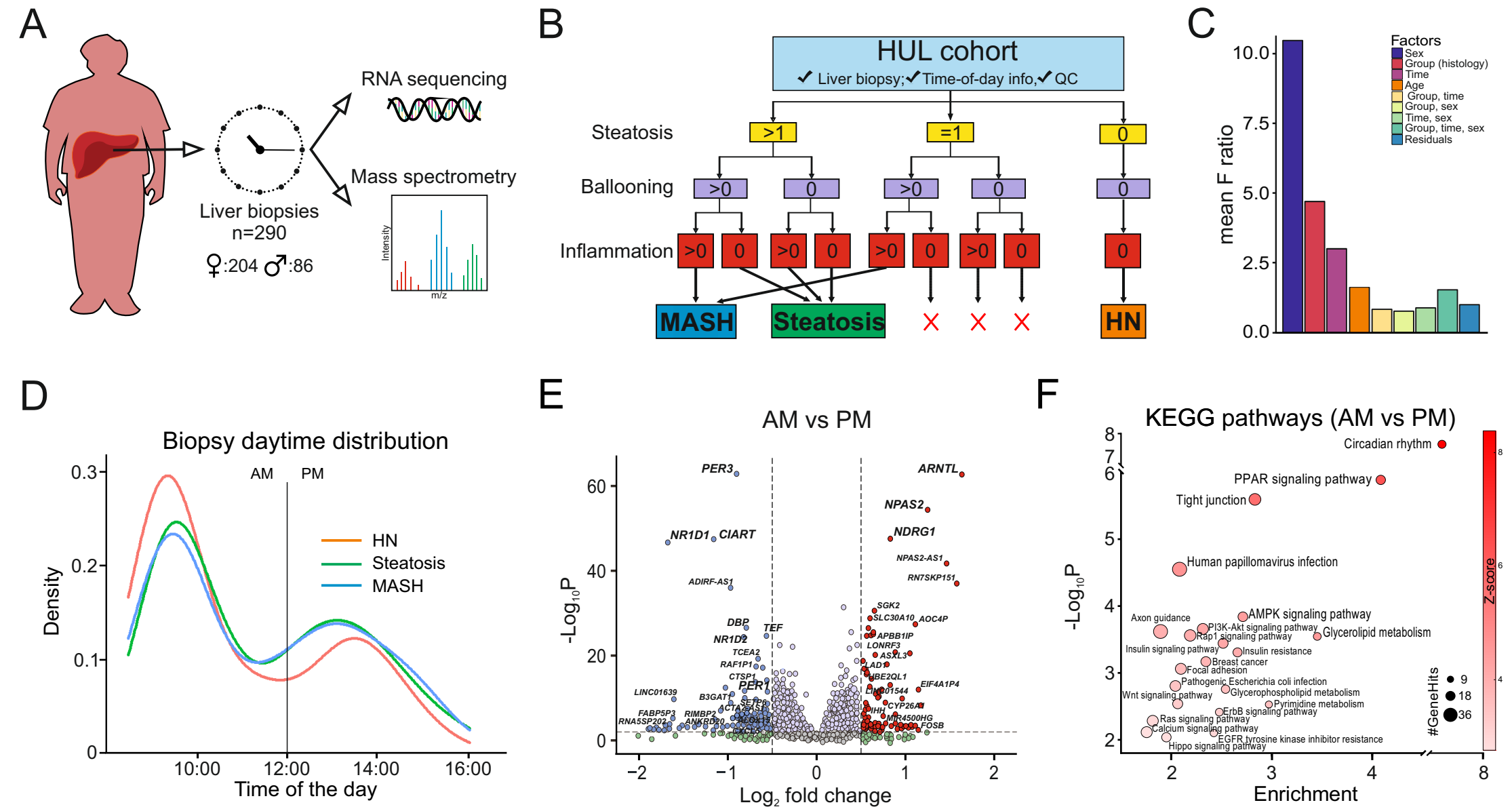


FIGURE 1_R2 - JOHANNIS et al.

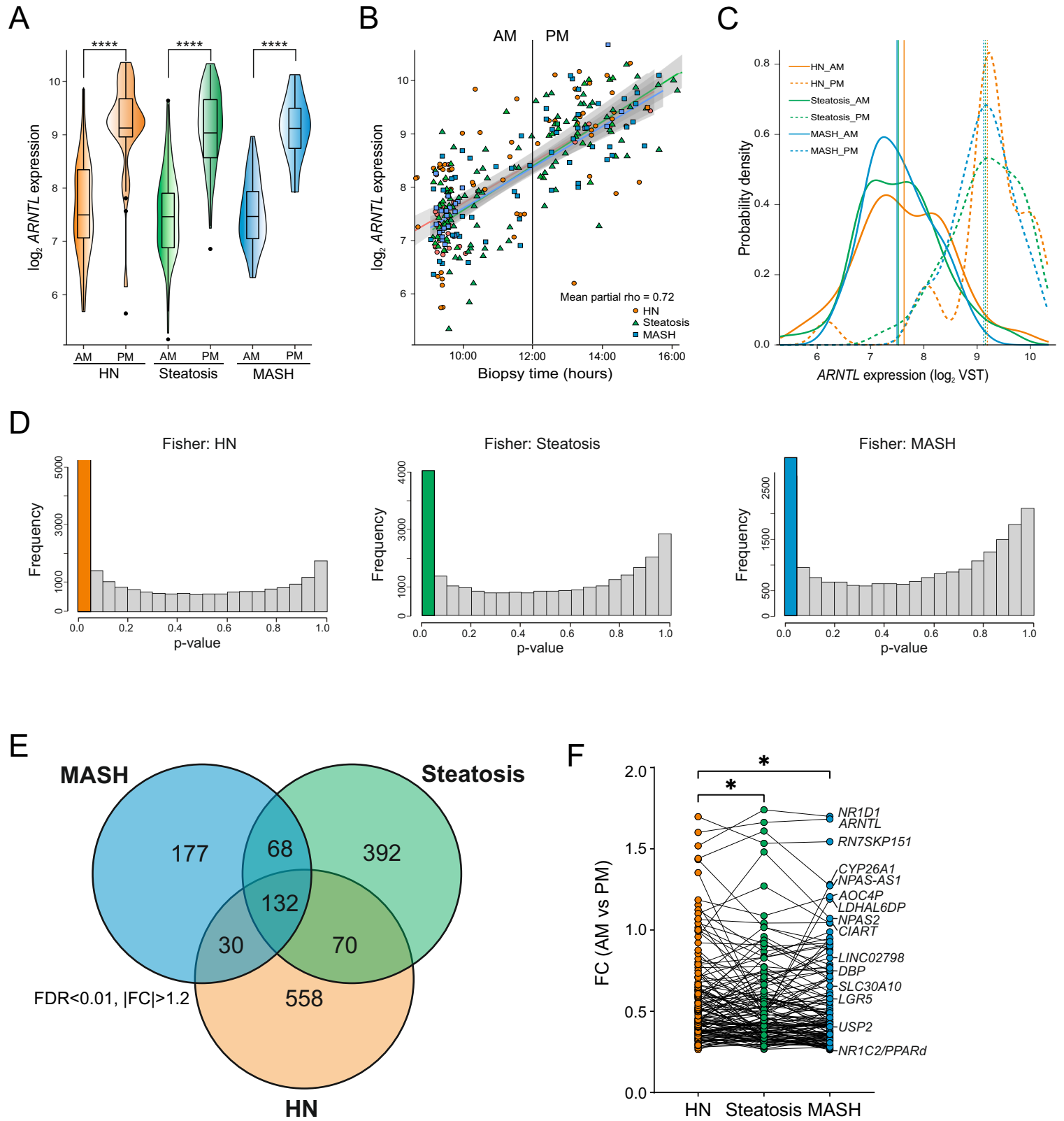


FIGURE 2_R2 - JOHANNNS et al.

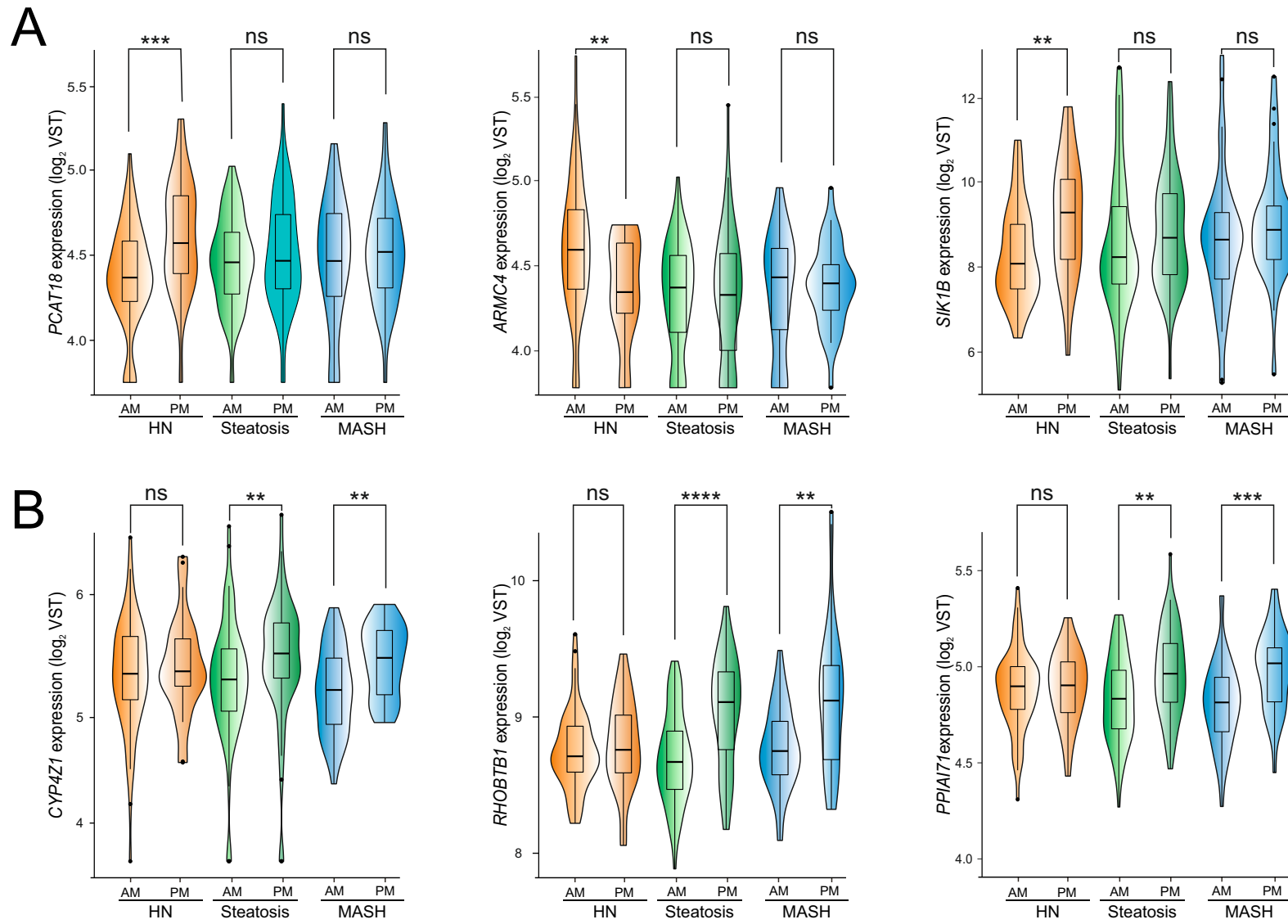
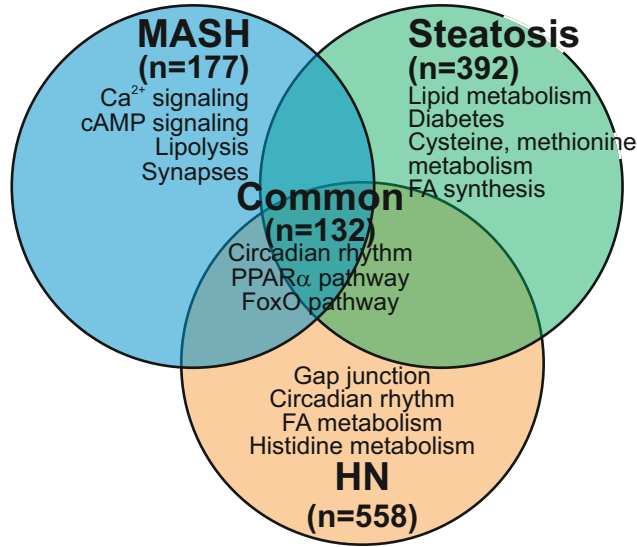
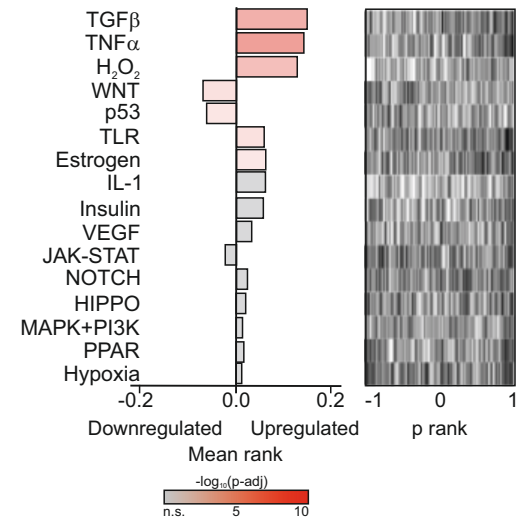


FIGURE 3_R2 - JOHANNIS et al.

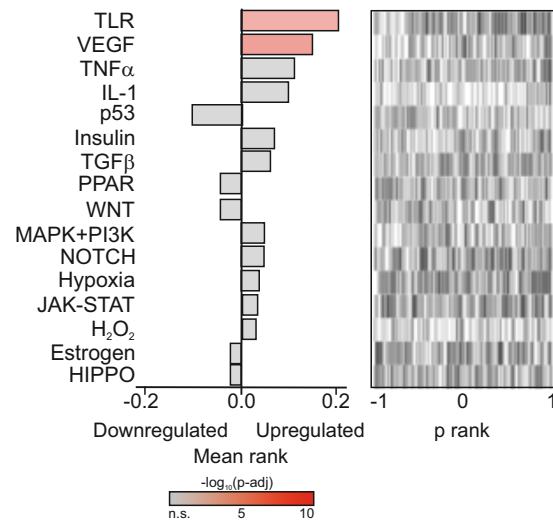
A) GO BP term enrichment



B) Pathway activity ranking (HN)



C) Pathway activity ranking (Steatosis)



D) Pathway activity ranking (MASH)

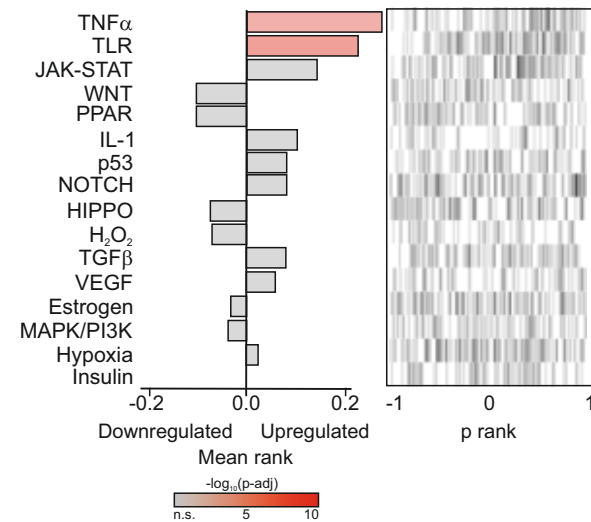


FIGURE 4_R2 - JOHANNNS et al.

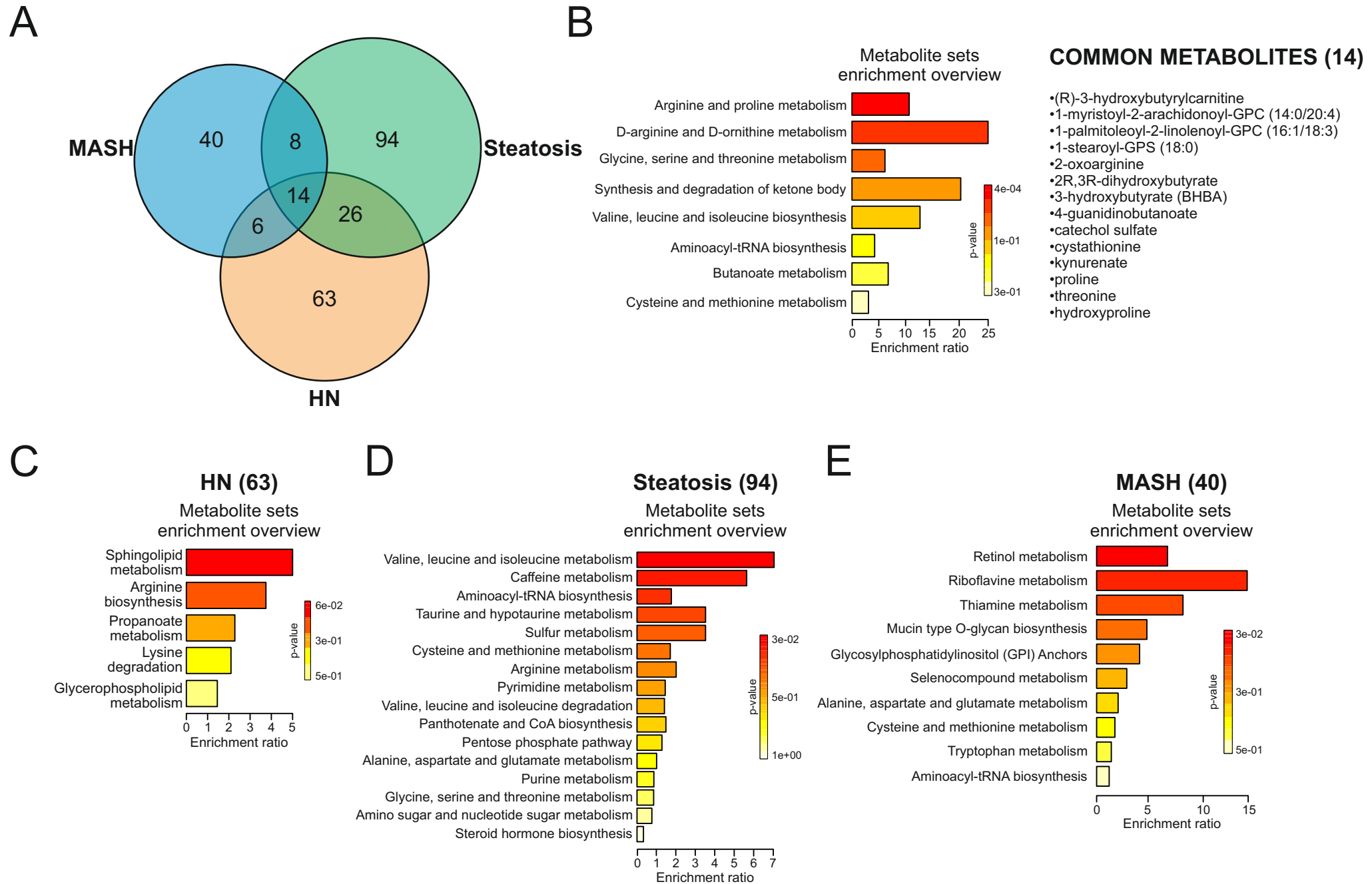


FIGURE 6_R2 - JOHANNNS et al.

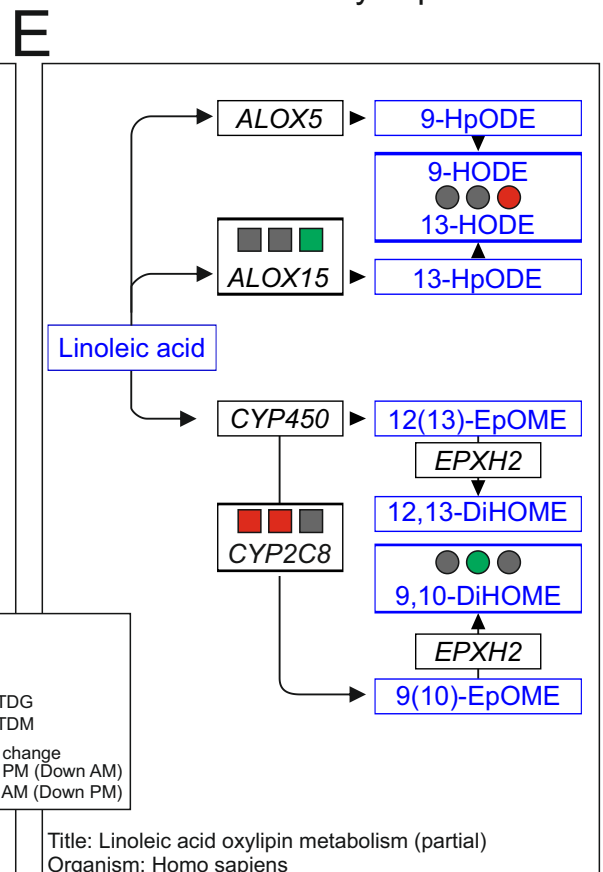
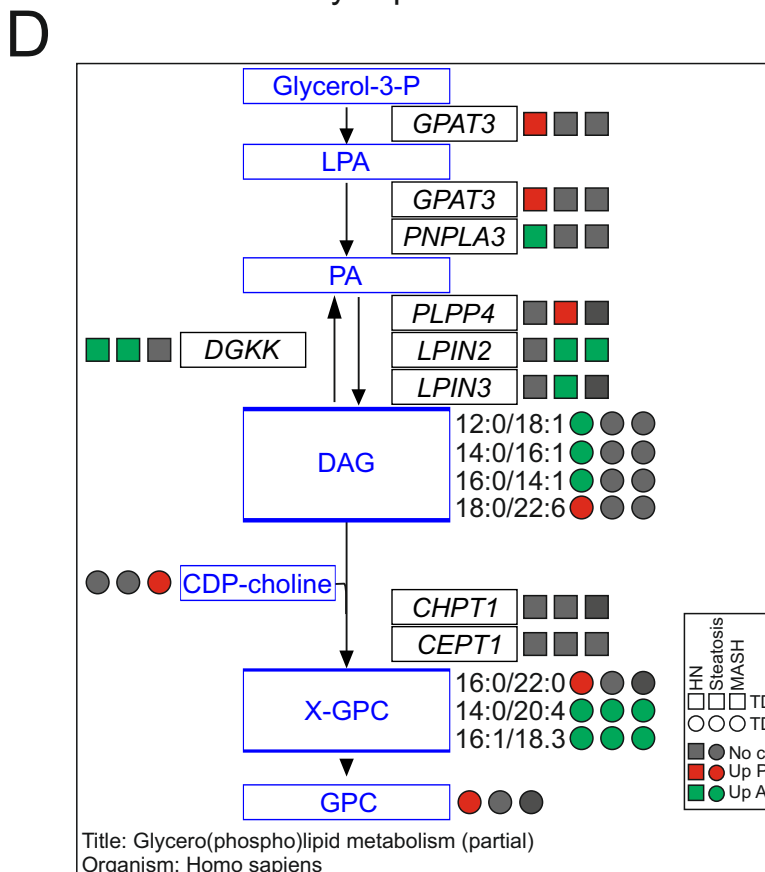
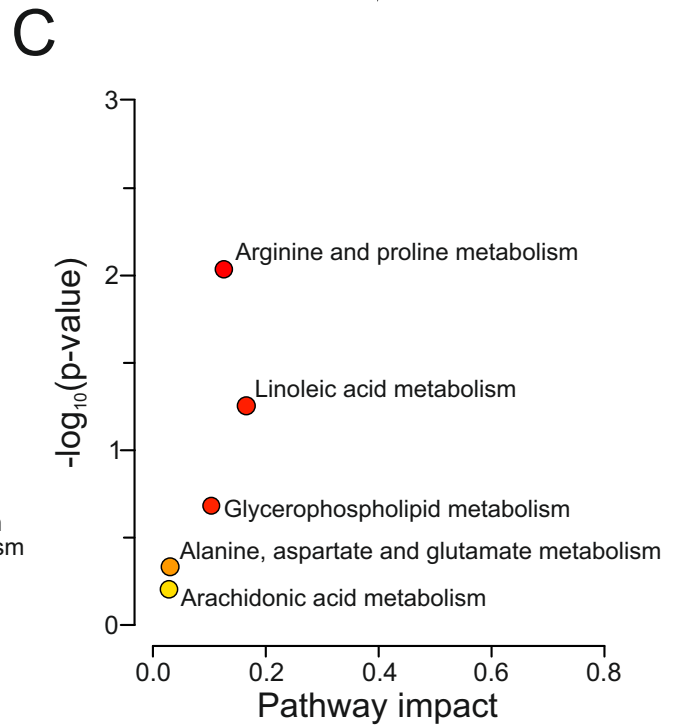
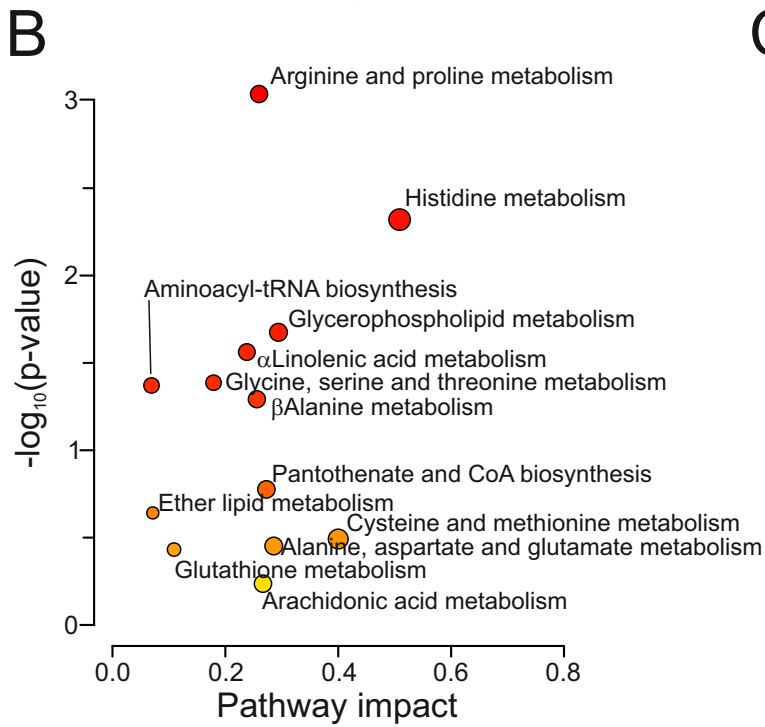
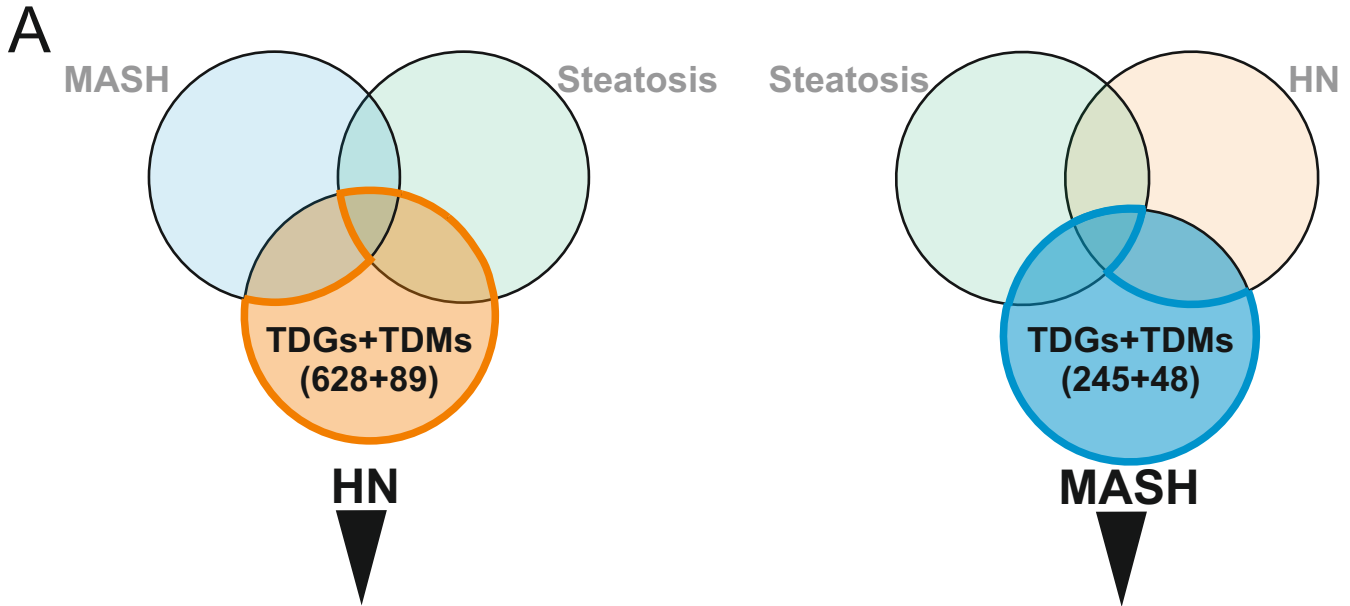


FIGURE 7_R2 - JOHANNNS et al.

Variable	N	MASLD Group			p-values		
		HN, n = 89	St. , n = 122	MASH, n = 79	HO vs. St.	HO vs. MASH	St. vs. MASH
Sex	290				0.003	0.008	0.7
F		75/89 (84%)	80/122 (66%)	49/79 (62%)			
M		14/89 (16%)	42/122 (34%)	30/79 (38%)			
Age	290	34.6 ± 11.4	41.8 ± 10.9	46.4 ± 10.4	<0.001	<0.001	0.050
BMI	290	45.4 ± 6.8	47.3 ± 7.9	46.2 ± 7.9	ns	ns	ns
Steatosis score	290				<0.001	<0.001	<0.001
0		89/89 (100%)	0/122 (0%)	0/79 (0%)			
1		0/89 (0%)	0/122 (0%)	18/79 (23%)			
2		0/89 (0%)	71/122 (58%)	29/79 (37%)			
3		0/89 (0%)	51/122 (42%)	32/79 (41%)			
Inflammation score	290				<0.001	<0.001	<0.001
0		89/89 (100%)	70/122 (57%)	0/79 (0%)			
1		0/89 (0%)	44/122 (36%)	55/79 (70%)			
2		0/89 (0%)	8/122 (6.6%)	23/79 (29%)			
3		0/89 (0%)	0/122 (0%)	1/79 (1.3%)			
Ballooning score	290				ns	<0.001	<0.001
0		89/89 (100%)	115/122 (94%)	0/79 (0%)			
1		0/89 (0%)	7/122 (5.7%)	57/79 (72%)			
2		0/89 (0%)	0/122 (0%)	22/79 (28%)			
Fibrosis score (Kleiner)	282				0.009	<0.001	<0.001
0		79/89 (89%)	78/118 (66%)	12/75 (16%)			
1		9/89 (10%)	28/118 (24%)	22/75 (29%)			
2		0/89 (0%)	7/118 (5.9%)	13/75 (17%)			
3		1/89 (1.1%)	5/118 (4.2%)	25/75 (33%)			
4		0/89 (0%)	0/118 (0%)	3/75 (4.0%)			
NAS score	290				<0.001	<0.001	<0.001
0		89/89 (100%)	0/122 (0%)	0/79 (0%)			
2		0/89 (0%)	40/122 (33%)	0/79 (0%)			
3		0/89 (0%)	51/122 (42%)	11/79 (14%)			
4		0/89 (0%)	26/122 (21%)	19/79 (24%)			
5		0/89 (0%)	5/122 (4.1%)	29/79 (37%)			
6		0/89 (0%)	0/122 (0%)	17/79 (22%)			
7		0/89 (0%)	0/122 (0%)	2/79 (2.5%)			
8		0/89 (0%)	0/122 (0%)	1/79 (1.3%)			
HOMA-IR	279	3.8 ± 4.8 ¹	13.5 ± 58.8 ¹	24.2 ± 55.2 ¹	<0.001	<0.001	<0.001
Biopsy time	290				ns	ns	ns
AM		62/89 (70%)	70/122 (57%)	46/79 (58%)			
PM		27/89 (30%)	52/122 (43%)	33/79 (42%)			

TABLE 1_R2 - JOHANNNS et al.